Temporal modulations of NODAL, BMP and WNT signals guide the spatial patterning in self-organized human ectoderm tissues

Tianfa Xie, 1,5, Jiming Kang^{2,5}, ChangHui Pak³, Hongyan Yuan², and Yubing Sun^{1,4,6*}

¹Department of Mechanical and Industrial Engineering, University of Massachusetts, Amherst, Massachusetts 01003, USA

²Department of Mechanics and Aerospace Engineering, Southern University of Science and Technology, Shenzhen 518055, China

³Department of Biochemistry and Molecular Biology, University of Massachusetts, Amherst, Massachusetts 01003, USA

⁴Department of Chemical Engineering, University of Massachusetts, Amherst, Massachusetts 01003, USA

⁵These authors contributed equally to this work

⁶Lead Contact

*Correspondence: ybsun@umass.edu (Yubing Sun)

KEYWORDS

Human embryonic stem cells, organoids, ectoderm, WNT, BMP, reaction-diffusion, neural crest, placode, mechanotransduction

SUMMARY

Developmental biology studies using model organisms suggest that the emergence of spatial patterning in the ectoderm is mediated by the morphogen gradients. However, it is still unclear whether morphogen gradient is necessary and dominates the cell spatial patterning, particularly in human genetic background. Here we demonstrate that human pluripotent stem cells can self-organize to concentric rings of all major cell types in ectoderm when cultured on micropatterned surfaces in a chemically defined condition. We reveal that modulating the dynamics of NODAL, BMP, and WNT signals is sufficient to control the spatial order of different cell types. Our mathematic model suggests that changes in wavelength and phase of signaling patterns formed via reaction-diffusion may be the mechanism by which temporal information is translated into spatial information. Together, our work demonstrates that *in vitro* human ectoderm microtissues have great potentials in understanding the mechanisms of early-stage human development.

INTRODUCTION

The development of the central nervous system begins from neural induction, during which the primitive ectoderm gives rise to neuroepithelium, neural crest, placodes, and epidermis. The regionalization of various cell types enables the precise localization of neural crest cells and placodes, which migrate from the dorsal end of the neural tube and form skull and cranial sensory organs, *etc.*, while epidermal cells cover the surface of embryos. A pivotal goal of neural development research is to identify the mechanism of this regionalization process¹.

Numerous studies using animal models (e.g., Xenopus, chick, and zebrafish) have established that FGF, BMP and WNT signaling pathways participate in neural induction since the pioneer works of Spemann and Mangold². The currently accepted, although highly debatable, 'default model' for the neural induction proposes that biomolecules (e.g., noggin, chordin) secreted by the organizer (primitive node in human) antagonize BMP signaling and prime ectoderm cells with neural fate³⁻⁵. Due to the existence of a gradient of BMP antagonists, the neural plate is specified to become neuroepithelium, while the border region subjected to intermediate BMP level is specified to become neural crest and placode, flanked by epidermis which requires the highest BMP level. Research over the past two decades has converged to the view that the neural induction process is more complex than described by this simple default model^{6, 7}. In particular, while the central role of BMP remains valid, new evidence suggests the functional roles of WNT and FGF signals in neural induction, which may act concomitantly with, or separately from direct BMP inhibition to regulate BMP activities^{3, 8}. Moreover, their functions may not be evolutionarily conserved⁸. For instance, WNT signaling upregulates BMP expression and promote epidermal fate in the chick embryos⁹. In contrast, WNT3a activation does not impair

neural induction in mouse embryos, mouse embryonic stem cells, and human pluripotent stem (hPS) cells¹⁰⁻¹². These findings collectively demonstrate that there is still a lack of fundamental understanding of how BMP, WNT, and FGF signaling interact and guide the cell patterning process, particularly in the context of human development.

While the prevailing approach in developmental biology research is to use animal models, it is well received that neurulation events in human and mouse differ in many respects¹³. Recent works have explicitly demonstrated the potential of using hPS cells cultured in 2D and 3D microenvironments to model key features of gastrulation¹⁴⁻¹⁶. We previously reported an *in vitro* neuroectoderm model by culturing hPS cells on micropatterned surfaces¹⁷. In that model, hPS cells near the border region of the micropattern spontaneously differentiated into neural plate border (NPB) cells, whereas cells in the center of the pattern differentiated into neuroepithelial (NE) cells under the dual Smad inhibition condition. We further revealed that such self-organization was dictated by biomechanical forces arisen from geometrical confinement. However, this model lacks epidermis and placodal cells, and how BMP and WNT signaling pathways work in conjunction with biomechanical forces to regulate cellular spatial patterning is still unclear.

Here we report a complete *in vitro* ectoderm model containing all the major cell types (neuroepithelium, neural crest, placodes, and epidermis) by fine-tuning biochemical signals under chemically defined culture conditions. Moreover, we found that changing the sequence of NODAL, BMP, and WNT signaling activation could modulate the spatial order of the rings consisting of neural crest and epidermis. A mathematic model based on reaction-diffusion was

developed to demonstrate how such temporal information was translated to spatial patterning. Together, our work suggests that the time-dependent reaction-diffusion of signaling molecules dictates the patterning of ectoderm, in contrast to a conventional morphogen gradient mediated patterning model. The *in vitro* human ectoderm microtissues provide an engineered and controllable experimental platform to investigate the functional role of individual genes and molecules in ectoderm development in human.

MATERIALS AND METHODS

Cell culture: Both SOX10 :: EGFP bacterial artificial chromosome hES cell reporter line (H9; WA09, WiCell; NIH registration number: 0062; female; generated by Dr. Lorenz Studer's lab¹⁸) and control human induced pluripotent stem (hiPS) cell line (male; generated from human primary T-cells using episomal reprogramming method) were cultured in Essential 8 growth medium on hES cell-qualified Geltrex (Thermo Fisher Scientific). Karyotyping and mycoplasma testing were performed routinely to ensure genomic integrity. After treatment with EDTA dissociation buffer (5 min at 37 °C), the cells were collected using a cell scraper (BD Biosciences), centrifuged (200 g for 5 min), and re-dispersed in Essential 8 growth medium supplemented with ROCKi (Y27632, 10 μM; Cayman Chemical) before cell seeding. The induction media are comprised of Essential 6 basal media, TGF-β inhibitor SB431542 (SB, Cayman Chemical; 10 μM), WNT agonist CHIR99021 (CHIR, Cayman Chemical), and BMP4 recombinant protein (Gibco). The media was changed every day. All cells were cultured at 37 °C and 5% CO₂.

Microcontact printing: Soft lithography was used to generate micropatterned polydimethylsiloxane (PDMS) stamps from negative SU8 molds that were fabricated using

photolithography. These PDMS stamps were used to generate micropatterned cell colonies using microcontact printing, as described previously¹⁹. Briefly, to generate micropatterned cell colonies on flat PDMS surfaces, round glass coverslips (diameter = 25 mm, Fisher Scientific) were spin-coated (Spin Coater; Laurell Technologies) with a thin layer of PDMS prepolymer comprising of PDMS base monomer and curing agent (10:1 w/w; Sylgard 184, Dow-Corning). PDMS coating layer was then thermally cured at 110 °C for at least 24 h. In parallel, PDMS stamps were incubated with a vitronectin solution (20 µg ml⁻¹, in deionized water) for 1 h at room temperature before being blown dry with a stream of nitrogen. Excess vitronectin was then washed away by distilled water and the stamps were dried under nitrogen. Vitronectin-coated PDMS stamps were then placed on top of ultraviolet ozone-treated PDMS (7 min, UV-ozone cleaner; Jetlight) on coverslips with a conformal contact. The stamps were pressed gently to facilitate the transfer of vitronectin to PDMS-coated coverslips. After removing stamps, coverslips were disinfected by submerging in 70% ethanol. Protein adsorption to PDMS surfaces without printed vitronectin was prevented by incubating coverslips in 0.2% Pluronic F127 solution (P2443-250G, Sigma) for 30 min at room temperature. Coverslips were rinsed with PBS before placed into tissue culture plates for cell seeding. For micropatterned cell colonies, PDMS stamps containing circular patterns with diameters of 200, 600, and 1000 µm were used. Immunocytochemistry: 4% paraformaldehyde (Electron Microscopy Sciences) was used for cell fixation before permeabilization with 0.1% Triton X-100 (Fisher Scientific). Cells were blocked in 10% donkey serum for 1 h at room temperature. Primary antibodies listed in Supplementary Table 1 were then used for protein detection. For immunolabelling, donkey-anti goat Alexa Fluor 488, donkey-anti rabbit Alexa Fluor 555, and donkey-anti mouse Alexa Fluor

647 secondary antibodies were used. Samples were counterstained with 4,6-diamidino-2-phenylindole (DAPI; Invitrogen) to visualize the cell nucleus.

Image analysis: Confocal images were collected with NIS-Elements AR software using Nikon A1 Resonant scanning confocal inverted microscope. Alexa Fluor 488 was excited with 488 nm laser line. Alexa Fluor 555 was excited with 561 nm laser line. Alexa Fluor 647 was excited with 640 nm laser line. 10× objective was used. Data analysis was performed using the NIS-Elements AR analysis software. All other phase contrast and fluorescence images of micropatterned cell colonies were recorded using an inverted epifluorescence microscope (Leica DMi8; Leica Microsystems) equipped with a monochrome charge-coupled device (CCD) camera. Images were first cropped using a custom-developed MATLAB program (MathWorks; https://www.mathworks.com/) to a uniform square with pattern centroids aligned. Cell colonies with multilayered cellular structures, due to inevitably inhomogeneous cell seeding, were excluded from data analysis. Fluorescence intensity of each pixel in cropped images was normalized by the maximum intensity identified in each image. These normalized images were stacked together to obtain average intensity maps. To plot average intensity as a function of distance from colony centroid, average intensity maps for circular cell colonies were divided into 100 concentric zones with equal widths. The average pixel intensity in each concentric zone was calculated and plotted against the mean distance of the concentric zone from colony centroid. From average intensity plots of cell lineage markers, values of the full width at half maximum (FWHM) were determined as the difference between the two radial positions at which the average fluorescence intensity of individual markers is equal to half of its maximum value.

Reaction-diffusion mathematical model:

The reaction-diffusion model proposed by Barrio *et al.* was adopted in this work to study the effect of the initial condition and the effect of temporal orders of signal activation on the spatial patterns²⁰. Because the studied patterns are axisymmetric, an axisymmetric two-dimensional form of the reaction-diffusion equation²⁰ is used in this study

$$\frac{\partial u}{\partial t} = D \left(\frac{\partial^2 u}{\partial^2 r} + \frac{1}{r} \frac{\partial u}{\partial r} \right) + au - cv - ar_1 uv^2 - r_2 uv$$

$$\frac{\partial v}{\partial t} = hD \left(\frac{\partial^2 v}{\partial^2 r} + \frac{1}{r} \frac{\partial v}{\partial r} \right) + cu + dv - d \frac{ar_1}{b} uv^2 + r_2 uv$$
(1)

The initial condition for the equation is:

$$u(r,0) = u_0(r),$$

$$v(r,0) = v_0(r) .$$

And the equation satisfies the Neuman boundary condition:

$$\frac{\partial u}{\partial r} = 0, r = R$$

$$\frac{\partial v}{\partial r} = 0, r = R$$

where u(r,t), v(r,t) are the concentrations of activator and inhibitor respectively, D is the diffusivity of the activator, h is the ratio between the diffusion coefficients, model parameters a, c, d, r_1 and r_2 in the reaction terms will be tuned so that Turing instability occurs. The following conditions must be satisfied for Turing instability to occur:

$$a + d < 0$$

$$ad + c^2 > 0$$

$$d + ah > \sqrt{4h(ad + c^2)}$$
(2)

To facilitate the process of tuning parameter values, we introduce two new parameters \tilde{d} and e to replace d and b in the inequations above via the equations below:

$$d = -\tilde{d}a$$

$$b = a\sqrt{\tilde{d} + e} \tag{3}$$

The inequations then become:

$$\tilde{d} > 1$$

$$e > 0$$

$$h > \left(\sqrt{e} + \sqrt{e + \tilde{d}}\right)^{2}$$
(4)

Turing instability conditions will be satisfied if the parameters are chosen to satisfy inequations (4). Using the planar wave assumption, the critical wavenumber at which the instability grows fastest is

$$k_{\rm cri} = \sqrt{\frac{d + ah}{2hD}} \tag{5}$$

Note that the critical wavenumber k_{cri} increases with the model parameter a that is associated with the level of activator production rate. Since the diffusivities of the signaling molecules remain constant, in our model analysis, we kept parameter values of D and h constant. For the modeling results, the spatial patterns of u(r,t) and v(r,t) were obtained by solving the nonlinear equations (1) using the finite difference method.

RESULTS

BMP induces epidermis in micropatterned cells

We previously demonstrated that dual Smad inhibition and a transient WNT activation led to the regionalization of Pax6+ neuroepithelial cells and Pax3+ neural plate border cells on micropatterned surfaces¹⁷. To achieve complete ectoderm with epidermal, neural crest, and placodal cells, it is necessary to further activate BMP and WNT signals²¹⁻²³. Thus, we sought to investigate whether adding BMP4 and a β -catenin stabilizer CHIR to fully defined E6 media supplemented with TGF- β inhibitor SB431542 (SB, 10 μ M) is sufficient to induce those cell

types (referred to henceforth as the "B.C.SB protocol", **Supplementary Fig. 1A**). As shown in **Fig. 1**, by continuously activating BMP and WNT signals, micropatterned (diameter, 600 μm) H9 human embryonic stem (hES) cells self-organized into structures with four distinct zones. We found that cells located in both the center and outermost rings of the pattern were CDX2+, indicating a trophoblast fate, in consistence with previous findings that BMP4 activation in the absence of FGF signaling can induce trophoblast differentiation^{24, 25}. In addition, we found that the layer next to the outer ring of trophoblasts expressed SOX10, PAX3, and SOX9, markers for neural crest cells²⁶. Cells expressing TP63 and E-cadherin (E-cad), epidermis markers^{27, 28}, were found between the SOX10+ PAX3+ SOX9+ cells and center CDX2+ cells. Using an independent control human induced pluripotent stem (hiPS) cell line, we observed similar spatial patterning of these cell types (**Supplementary Fig. 2**).

As CDX2 signals in the center and edge of the micropatterns needed to be collected at different focal distances, we used confocal microscopy to further characterize the three-dimensional cytoarchitecture in micropatterns. Confocal images of nuclei staining suggested that micropatterned cells formed a dome-shaped monolayer with colony thickness less than 22 μm (Supplementary Fig. 3). Importantly, we did not find cells co-expressing TP63 and SOX10, suggesting the separation of cells with neural crest and epidermal fates. In addition, CDX2 confocal images confirmed that these trophoblast-like cells occupied the center and the outermost region of the colony (Supplementary Fig. 4). We further examined the existence of placodal cells and found that AP2+ SIX1+ placodal cells^{22, 29} mainly located in the ring containing SOX10+ neural crest cells (Supplementary Fig. 5), suggesting that under this condition, the neural crest cells and placodal cells were not separated yet. To examine whether the localization of the putative neural crest/placodes and epidermis is a result of cell sorting, we

immunostained TP63 and SOX10 at day 5, 6, and 7 of the differentiation (**Supplementary Fig.**6) and found that both TP63+ and SOX10+ cells emerged at day 6 with the same localization.

These results are consistent with our previous findings in neuroectoderm patterning and suggest that cell migration or cell sorting is not the major driving force for such pattern formation.

Effects of initial seeding density and pattern size on cell regionalization

We next sought to investigate whether the initial seeding density could affect the cytoarchitecture of the patterned cells by plating cells under three different seeding densities (40,000 cell cm⁻², 80,000 cell cm⁻² and 160,000 cell cm⁻²). Interestingly, we found a gradual shift of both the TP63+ and SOX10+ cells towards the border of the circular patterns with increasing seeding density (**Fig. 2A, B**). The average intensity peaked at 81, 152, 260 μm from the pattern center respectively for TP63 and 158, 184, 259 μm respectively for SOX10 when the seeding density increased from 40, 000 to 160,000 cell cm⁻² (**Fig. 2C**).

We also examined the effect of pattern size on the spatial patterning of the ectoderm microtissue *in vitro* (**Fig. 3**). To this end, we generated circular adhesive islands with diameters of 200, 600 and 1000 μm. In contrast to our previous finding, which showed that the neuroepithelium-neural plate border two-layer patterning is insensitive to pattern size, in this condition, patterns with a diameter of 200 μm failed to produce intact rings of TP63+ cells. For 1000 μm patterns, TP63+ cells or SOX10+ cells did not form an intact ring either and the boundaries between TP63+ cells and SOX10+ cells were not as distinct as in 600 μm patterns, as reflected by the overlapping peak of intensities (324 μm *vs* 342 μm). Noticeably, in all these conditions, we did not observe any cell co-expressing TP63 and SOX10 by examining the merged images, and the relative localization of TP63+ and SOX10+ rings remained unchanged.

Reaction-diffusion models predicted the pattern formation

We previously described a mechanics-driven model to explain the formation of the two-layer neuroectoderm microtissues, based on the distinct mechanical status of cells at the center and periphery of the patterns¹⁷. However, the observed patterns here were significantly different because of the existence of apparent periodic structures (two CDX2+ layers), and the sensitivity to pattern size. Thus, a simple mechanical or chemical gradient was not sufficient to explain the formation of such complex structures. Moreover, the observed relative localization of epidermis and neural crest/placodes is opposite to the ectoderm development in vivo, suggesting such pattern formation is not solely autonomous and is strongly affected by external chemical signals. Thus, we aimed to develop a theoretical model to explain these observations, and predict under what conditions, the order of epidermis and neural crest/placodes can be reversed to mimic ectoderm development in vivo. To simplify the model, we first hypothesized that BMP and WNT signals do not strongly crosstalk with each other, and the cell fate depends on the synergistic effects of BMP and WNT activities. BMP4-Noggin and WNT-Dickkopf (DKK) are two wellestablished activator-inhibitor pairs^{30, 31}, and cell-secreted proteins from the micropatterned cells can rapidly diffuse to the culture media³⁰. For such systems, the classic Turing's reactiondiffusion model³² predicts the presence of periodic activities of BMP and WNT signals (Fig. 4A). We found that to achieve the four-layer patterns we observed in Fig. 1 and Supplementary Fig. 2, one would expect periodic high and low BMP and WNT activities with a similar wavenumber (reflected by the number of regions within each pattern) but a phases shift (i.e., the sequence of high or low level of signals) within the pattern (Fig. 4A, B).

We next sought to understand what factors can be used to tune the phase and wavenumber in this system. We adopted an axisymmetric two-dimensional form of the reaction-diffusion model, and

specifically studied the effect of individual parameters on the growth of Turing instability. A brief description of the mathematical model and model calculations are given in the MATERIALS AND METHODS section above. We first found that with constant diffusivities, the phase of the patterns can be reversed by changing the initial conditions of the partial differential equations. Our simulation results in **Fig. 4C** show that the phase is sensitive to a subtle change in initial conditions. Further, we demonstrated that the wavenumbers in the circular domain could be varied by changing the parameter value of a only. As shown in **Fig. 4D**, the value of a = 0.3078 leads to a simple Low-High pattern (two regions), a value of a = 0.6156 leads to three regions, while a = 1.5390 yields four regions. Noticeably, the parameter a represents the coefficient of the production rate of the activator (e.g., BMP). Our theoretical analysis strongly suggests that the number of the regions and order of cell types in each region can be tuned by changing the initial condition and the level of BMP/WNT activators.

Effects of BMP/WNT activation starting time

Based on the theoretic model we proposed, to derive intact ectoderm microtissues with proper regionalization of neuroepithelium, neural crest/placodes, and epidermis, a possible way is to reduce the number of layers in the pattern from three to two, and synchronize the phase of BMP and WNT patterns (**Fig. 4E**). This might be achieved by lowering the activities of exogenous activators and changing the initial conditions as suggested by the model. To test this possibility, we first modified the B.C.SB protocol (**Supplementary Fig. 1B**) to delay the starting time for BMP and/or WNT activation from day 3 to day 5, which effectively reduced the initial signaling activations (*i.e.*, a smaller *a* value in our model) and also changed the initial conditions. We found that when both BMP and WNT signal activation was delayed, we could obtain a three-layer structure with Pax6+ neuroepithelial cells in the center of the pattern, flanked by SOX10+

PAX3+ SOX9+ neural crest cells. A significant amount of TP63+ E-cad+ epidermal cells were located on the border of the pattern (Fig. 5 for H9 cells and Supplementary Fig. 7 for control hiPS cells), and only a very small number of CDX2+ cells were found in the outermost region of the patterns. This agrees with the model prediction that both BMP and WNT activities need to be tuned down. In contrast, solely delaying the activation of WNT signals led to a three-layer structure with neural crest cells located on the border of the pattern, and TP63+ cells located on the inner side of the SOX10+ cells. The number of Pax6+ cells also significantly decreased in the pattern center (Fig. 5, Supplementary Fig. 7). Solely delaying the activation of BMP signals, however, completely disrupted the ring shape pattern formation and largely inhibited neuroepithelial cell differentiation (Fig. 5, Supplementary Fig. 7).

Dosages of BMP and WNT activators regulate cell fate decision but not regionalization

We next examined whether modulating the concentration of BMP and WNT activators could also affect the relative localization of different cell types. By changing the dosage of BMP4 added to the culture media using the B.C.SB protocol, we found that the exogenous BMP4 concentration strongly influenced the neural crest and epidermal differentiation (**Fig. 6**). When BMP4 was not added, epidermis differentiation was completed inhibited, and neural crest differentiation was also significantly reduced, resulting in incomplete ring structures. A low concentration of BMP4 (1 ng·ml⁻¹, compared with 5 ng·ml⁻¹ for the optimal condition shown in **Fig. 1**) also failed to induce an intact ring of TP63+ cells while strongly promoting neural crest differentiation, as the full width at half maximum (FWHM) for spatial distributions of SOX10 intensity increased from 84 μm for 5 ng·ml⁻¹ to 280 μm for 1 ng·ml⁻¹ (**Fig. 6C**). A high concentration (20 ng·ml⁻¹) of BMP4 prohibited neural crest differentiation and strongly promoted epidermis differentiation, and both cell types spread randomly on the patterns. In

contrast to BMP4, the concentration of CHIR has only marginal effects on ring formation (**Fig.** 7). Without WNT activation, we could still observe both TP63+ and SOX10+ rings of cells located in the same order as shown in **Fig. 1A**. However, a high concentration of CHIR (1200 nM) led to the widespread morphology of the cells and inhibited epidermal differentiation. A much higher concentration of CHIR (3 µM) completely inhibited both epidermal and neural crest differentiation (**Fig. 7**). Although changing the concentrations of BMP or WNT activator can significantly influence the differentiation potential, we did not observe the change of relative localization between epidermis and neural crest cells. Together, our results here showed that the absolute concentrations of BMP and WNT mainly affect the width of each ring of different cell type, without changing their relative position.

Generation of complete ectoderm in vitro

By delaying the starting point of BMP and WNT activation, we successfully synchronized the phases of BMP and WNT patterns. The hPS cells generated ectoderm-like structures with neuroepithelial cells in the pattern centers, although the neural crest and epidermis layers were not completely separated (**Fig. 5 and Supplementary Fig. 7, top panels**). In addition, changing the concentration of exogenous BMP4 and WNT activator could regulate the width of each ring without affecting their relative locations (**Fig. 6, 7**). Thus, we asked whether a combination of these two approaches, *i.e.*, simultaneously changing the BMP4 initial concentration and delaying its activation start time, could lead to a more accurate ectoderm *in vitro* model. We further modified the B.C.SB protocol (**Supplementary Fig. 1B**) to reduce the concentration of BMP4 from 5 ng/ml to 1 ng/ml or increase to 40 ng/ml. We found that when BMP4 concentration was reduced, hES cells formed a three-layer structure with Pax6+ neuroepithelial cells in the center of the pattern, flanked by a layer of SOX10+ SOX9+ PAX3+ neural crest cells, and then another

layer of TP63+ E-cad+ epidermis. Only a negligible amount of CDX2+ cells were located on the border of the pattern (**Fig. 8A-B**, **top panels**). In contrast, higher concentration of BMP4 led to a three-layer structure with a significant amount of CDX2+ cells located on the border of the pattern, PAX6+ neuroepithelium in the center, and a mixed population of neural crest and epidermis cells between trophoblast and neuroepithelium (**Fig. 8A-B**, **bottom panels**). Together, these results suggested that the time-dependent reaction-diffusion of signaling molecules dictates the patterning of ectoderm (**Fig. 8C**). The *in vitro* complete human ectoderm microtissues we generated may facilitate the study of human ectoderm development ate the cellular and molecular levels.

DISCUSSION

In vitro differentiation of micropatterned hPS cells has become a powerful tool for studying early-stage of human development including gastrulation and neurulation^{14, 17, 28, 30, 33, 34}. A common observation in these reported systems is the formation of concentric rings of cells with different fates. It remains unclear how such self-organization process is regulated, as both mechanical states and reaction-diffusion mechanisms have been proposed^{17, 30}. Our results and mathematical models here suggest that the dominance of the reaction-diffusion mechanism can be tuned by exogenous signals. Our previous work showed that under the BMP4 inhibition condition (*i.e.*, very small a value in our model), only two cell layers were observed, and intrinsic BMP activations were controlled by mechanical states of cells¹⁷. When exogenous BMP and/or WNT are provided, the cell fate patterning cannot be explained solely by mechanics because otherwise epidermis, which requires the highest level of BMP4 activation, should always locate on the border of the pattern, where largest mechanical forces are located. The difference in the sensitivity to pattern size also supports this argument. The cell regionalization is

insensitive to pattern size when mechanics dominates the process. When the reaction-diffusion becomes the dominating mechanism, the pattern size becomes a critical factor³⁰. Similarly, the conventional 'default model' claiming that the diffusion of BMP4 or its antagonist patterns the ectoderm might be viewed as a special case in the reaction-diffusion model when the a value is small. With a high level of exogenous BMP and WNT, the simple diffusion model cannot explain the existence of periodic structures (CDX2+ cells in the center and periphery of patterns) and reversible order of epidermis and neural crest cells found in our system (Fig. 1, and Fig 5). Our analysis suggests that the number of zones and the relative localization of each zone are likely determined by the wavenumbers and phases of the reaction-diffusion patterns, which can be modulated by initial condition and activator production rate. Notably, our model assumes that BMP and WNT signals act independently. It has been found that Wnt3a can temporarily upregulate BMP4 expression and induce neural crest³⁵ and epidermal fates⁹ in chick embryos. Therefore, a more sophisticated model that incorporates this crosstalk is needed to quantitatively explain the experimental observations, such as the effects of colony size and cell seeding density. However, as both BMP and WNT activation are required for the neural plate specification and epidermal differentiation^{36, 37}, and BMP and WNT activities in our system are dominated by exogenous activators, in this system it may still be reasonable to assume the crosstalk between BMP and WNT is minimal. Indeed, our model successfully described the spatial patterning of different cell types under different initial conditions. Together, our studies reveal that the exogenous levels of BMP and/or WNT is responsible for the switching between different patterning mechanisms.

The existing theories in developmental biology often attribute the pattern formation to the existence of a persistent spatial morphogen gradient. Our results, however, suggest a "temporalspatial" mechanism as an alternative to the conventional "spatial-spatial" mechanism. Specifically, the relative location of these rings could be tuned by changing the order of NODAL inhibition (by SB) and BMP4 activation. NODAL inhibition was required prior to BMP4 activation to acquire neuroepithelium, which always located in the center of the pattern. Also, WNT activation is not required for the formation of ring-like structures, because the ring shapes could still form when CHIR was either completely removed (Fig. 7) or added two days later (Fig. 5, the middle row). Interestingly, if WNT activation was not accompanied by BMP4 activation (Fig. 5, the bottom row), it prevented the formation of ring-like structures. In contrast, the exogenous BMP4 level has to be in a very narrow range (1-20 ng·ml⁻¹) and BMP4 has to be activated no later than WNT (Fig. 5, 6) to initiate the ring shapes. Together, these analyses suggest that NODAL inhibition, BMP4 activation, and WNT activation need to happen in sequence to obtain proper spatial patterning. In other words, the spatial patterning of cell fate is mediated by the temporal patterning of these signals. Our mathematical model implies the basic principle behind this "temporal-spatial" regulation: the temporal activation of different signaling can influence both phase and wavenumber of reaction-diffusion patterns of these signaling molecules. While the wavenumber can be modulated by both the timing and concentration of morphogens, the phase is mainly regulated by the timing, and thus changing the concentration of BMP/WNT activators could not reverse the relative localization of the rings. The temporal patterns of BMP4 and WNT activation have been studied in *Xenopus* and chick embryos. In *Xenopus*, the initial inhibition of WNT signaling was found to be required to specify the neural plate border fate³⁸. However, in chick embryo, the activation of WNT signaling precedes BMP

activation in order to generate neural plate border cells³⁵. Our results suggest that likely during human ectoderm development, the activation of BMP4 precedes or happens simultaneously with WNT signal activation, similar to the *Xenopus* model.

Various *in vitro* systems, including monolayer cell culture³⁹⁻⁴¹, neural rosettes^{39, 42, 43}, neural spheroids⁴⁴, and brain organoids⁴⁵⁻⁴⁹ have been developed to model neuronal development using pluripotent stem cells. Recently, Brivanlou and colleagues²⁸ and Warmflash and colleagues³³ also reported a similar self-organizing ectoderm or "neuruloids" model using hPS cells. Although the differentiation protocols of these two systems are slightly different, both require a delayed BMP activation, which agrees with our findings. Noticeably, the neuruloids models derived by the Brivanlou and colleagues were induced using mouse embryonic fibroblasts conditioned media supplied with a high concentration of BMP4 (50 ng·ml⁻¹), and did not require WNT activation or inhibition. Our protocol is based on completely defined E6 culture media, and thus uniquely revealed the collaborative roles of BMP and WNT signals and the precise range of required BMP4 protein. Thus, our chemically defined ectoderm *in vitro* model is more suitable for studying the signal transduction and interactions during the neurulation process.

In summary, in this work, we demonstrated how temporal order of signaling activation contributes to spatial patterning of the epidermis, neural crest cells and neuroepithelium in an *in vitro* ectoderm model. This is possibly due to the change of the wavelength and phase of the reaction-diffusion of the signaling molecules, leading to different modes of signal overlap, which correspond to different cell fate. As a chemically defined culture condition was used, our system can provide tremendous insights into the molecular signatures of the ectoderm development in

the human genetic background. Although our reaction-diffusion model can qualitatively explain the patterns we found, future works are still needed to fully understand how the phase is controlled, and how WNT-BMP crosstalk can be incorporated into the model.

FIGURES AND CAPTIONS

Figure 1

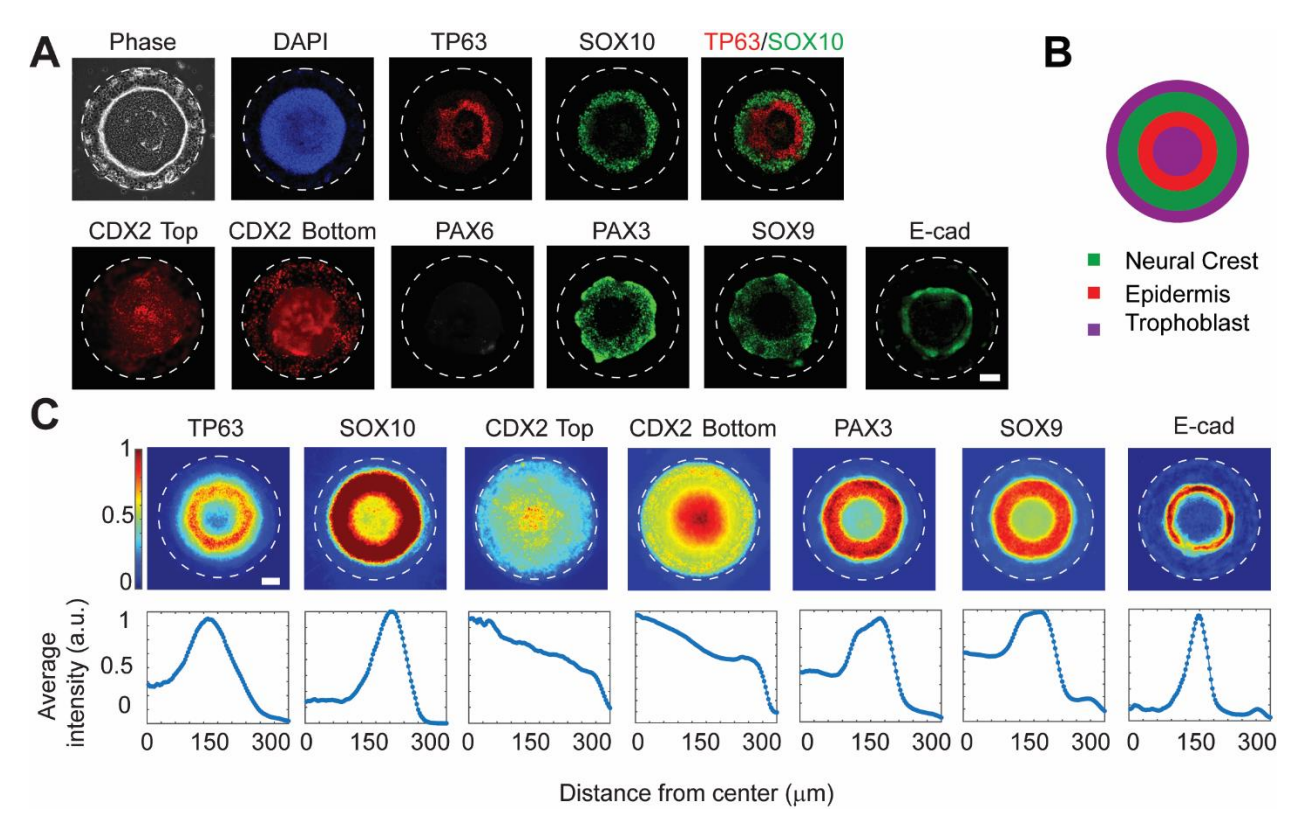


Figure 1. Self-organized ring shape structures of neural crest and epidermis formed on micropatterned substrates. (**A**) Representative phase and fluorescence images showing cell nuclei (DAPI), neuroepithelial cells marker (Pax6), neural crest markers (SOX10, PAX3, SOX9), epidermis marker (TP63, E-cad), and trophoblast marker (CDX2). For CDX2, fluorescence microscopic images were shown to visualize the top and bottom of the micropatterned cells, respectively. (**B**) A schematic shown the spatial distribution of all the cell types identified. (**C**) Top panel: colorimetric maps showing the average fluorescent intensity of SOX10, TP63, CDX2, PAX3, SOX9, and E-cad staining. The intensity of each pixel of the images was normalized to the maximum value for each image. n > 20. Bottom panel: Plots showing the quantitative average intensity in relation to the distance to the center of the pattern.

In these experiments, H9 hES cells were induced using the B.C.SB. protocol in E6 medium from day 3 to day 8. Scale bar, $100~\mu m$.

Figure 2

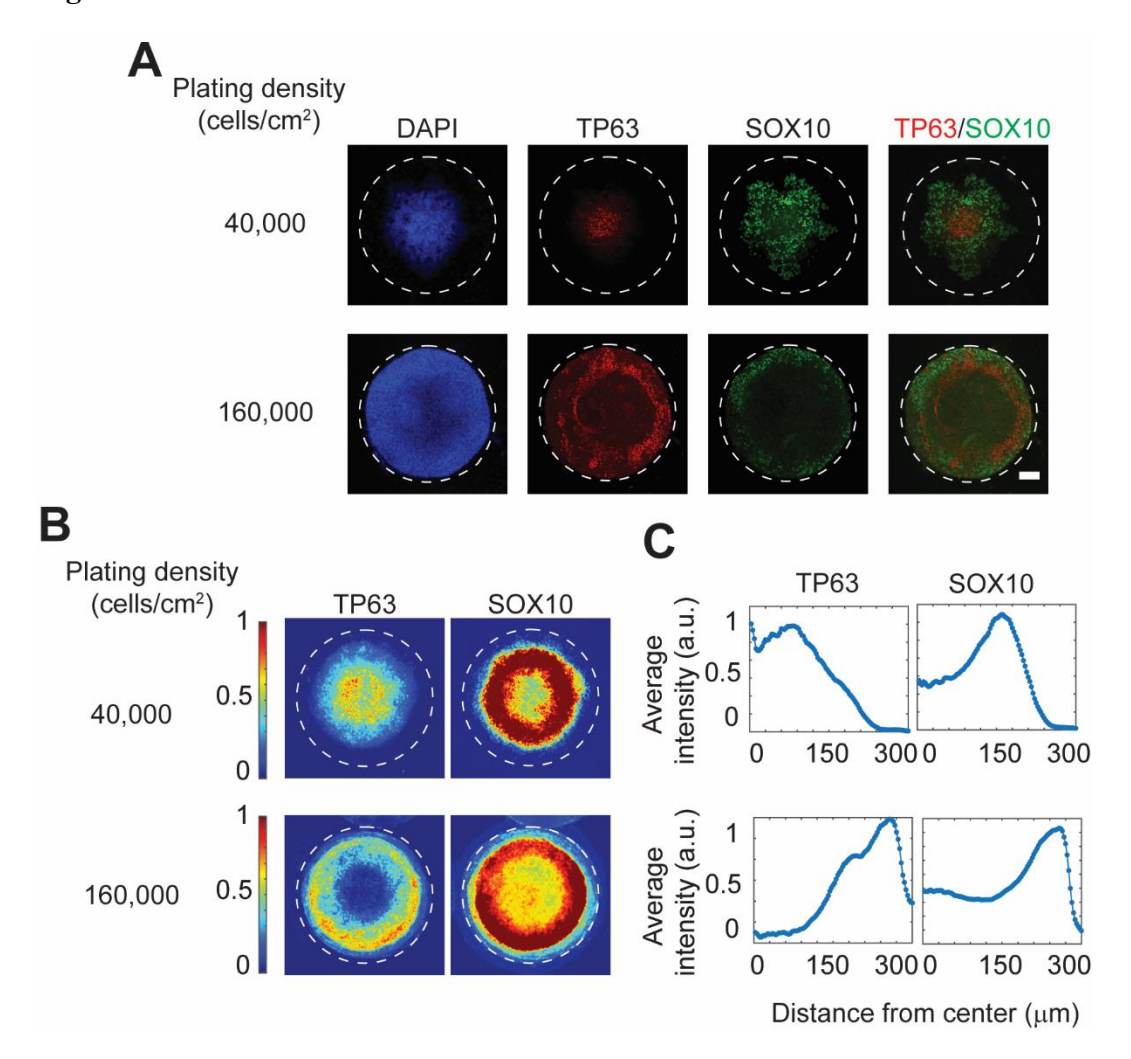


Figure 2. The effects of initial plating density on cell fate determination and neural crest and epidermis pattern formation in self-organized ectoderm tissue. (A) Representative fluorescence images showing cell nuclei (DAPI), neural crest marker (SOX10), and epidermis marker (TP63). The cells were plated onto micropatterned substrate at low (40,000 cells/cm²) or high density (160,000 cells/cm²). (B) Colorimetric maps showing the average fluorescent intensity of SOX10 and TP63 staining. The intensity of each pixel of the images was normalized to the maximum value for each image. n > 20. (C) Plots showing the quantitative average intensity in relation to the distance to the center of the pattern. In these experiments, H9 hES

cells were induced using the B.C.SB. protocol in E6 medium from day 3 to day 8. Scale bar, 100 $\,$ $\mu m.$

Figure 3

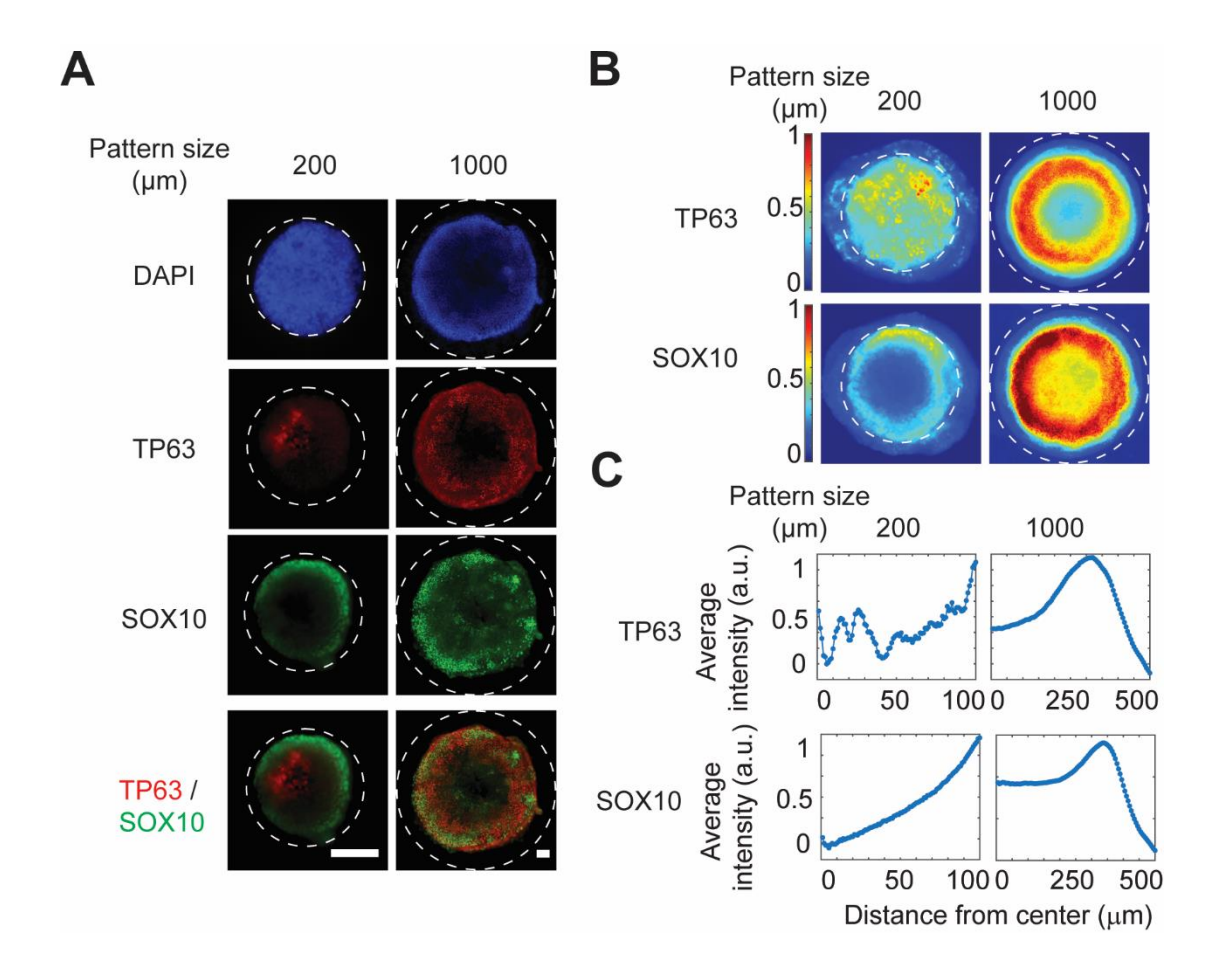


Figure 3. The effects of pattern size on cell fate determination and neural crest and epidermis pattern formation in self-organized ectoderm tissue. (A) Representative fluorescence images showing cell nuclei (DAPI), neural crest marker (SOX10), and epidermis marker (TP63). The cells were micropatterned with different pattern sizes as indicated. (B) Colorimetric maps showing the average fluorescent intensity of SOX10 and TP63 staining. The intensity of each pixel of the images was normalized to the maximum value for each image. n > 20. (C) Plots showing the quantitative average intensity in relation to the distance to the center of the pattern. In these experiments, H9 hES cells were induced using the B.C.SB. protocol in E6 medium from day 3 to day 8. Scale bar, 100 µm.

Figure 4

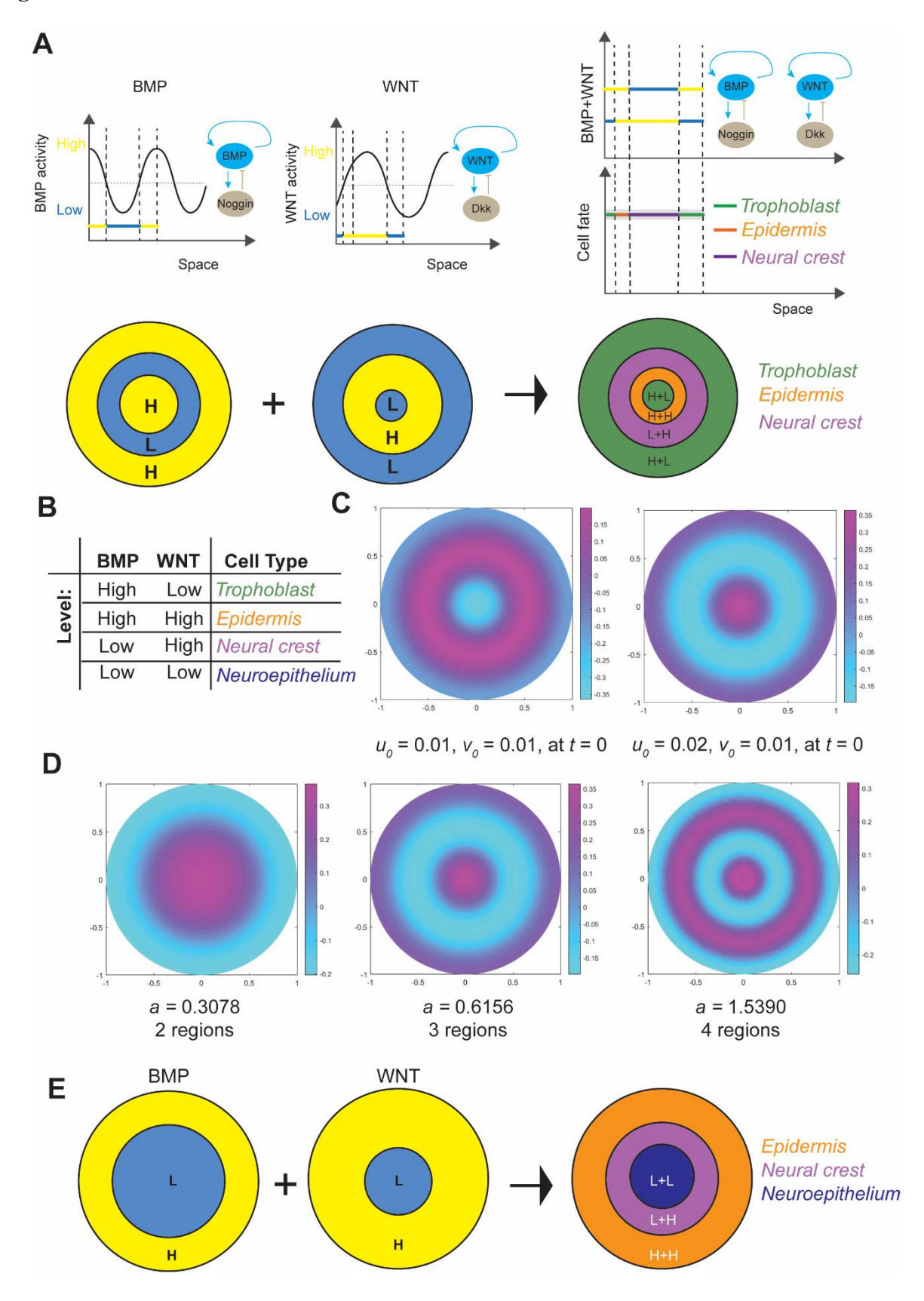


Figure 4. Reaction-diffusion model for pattern formation. (A) A schematic showing the activator-inhibitor pairs in the reaction-diffusion model and the hypothesized pattern of BMP and WNT activities. H: high activity L: low activity. A slight phase shift is assigned to the WNT pattern so that the central region is smaller than that of the BMP pattern. (B) A table showing cell fate as determined by the combination of BMP and WNT activities. (C) Simulation results showing the steady-state concentration distributions of the activator computed from the reaction-diffusion model with different initial conditions. (D) Simulation results showing the steady-state concentration distributions of the activator as a function of the model parameter a, representing the coefficient of the production rate of activator generation. (E) A schematic showing a possible way to generate three-layer structures with ectoderm-mimicking cytoarchitecture. Again, a phase shift is assigned to the WNT pattern compared with the BMP pattern.

Figure 5

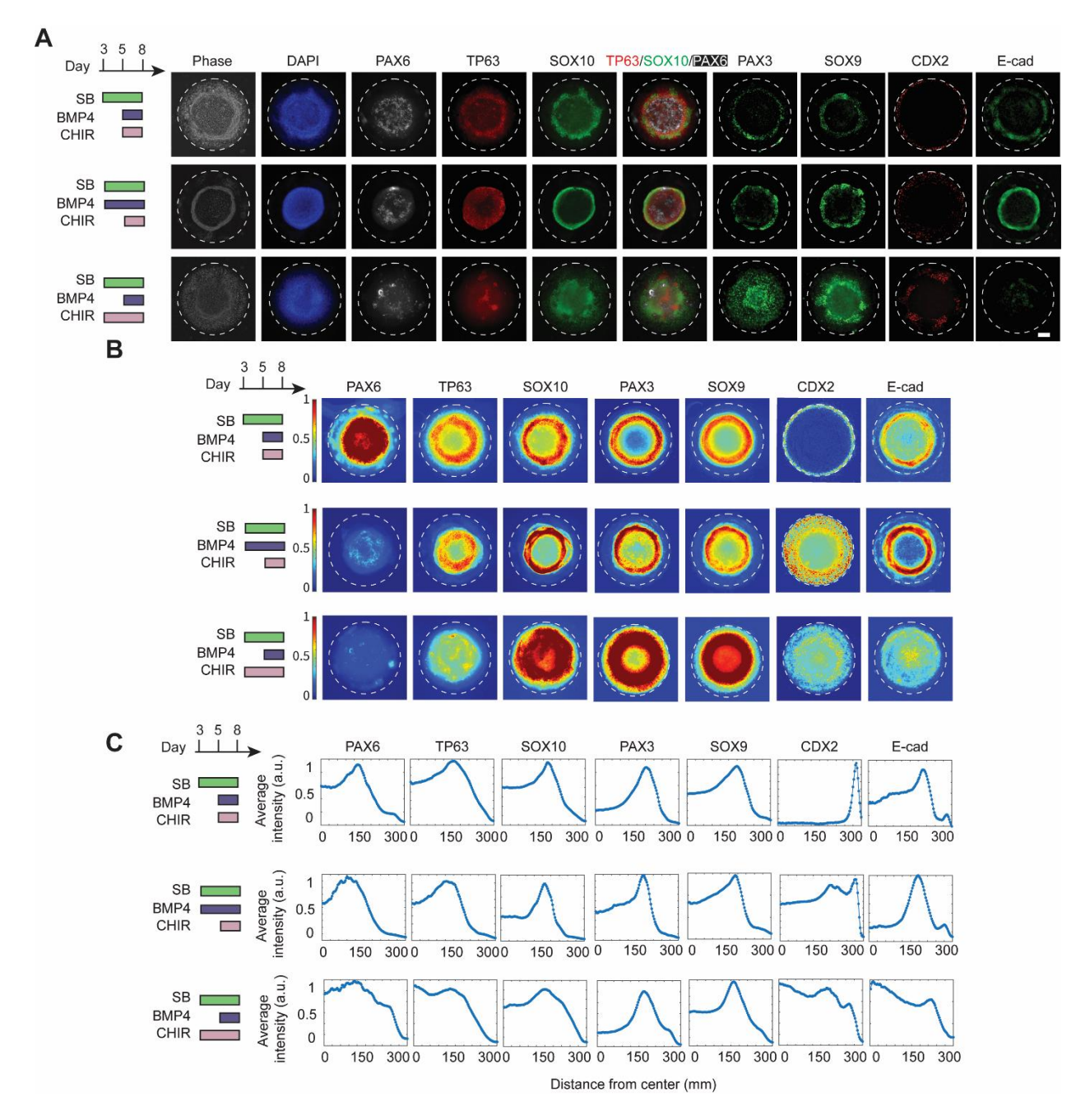


Figure 5. The effects of the activation starting time of BMP and WNT signals on the pattern formation in ectoderm microtissues. (A) Representative phase and fluorescence images showing cell morphology, nuclei (DAPI), neuroepithelial cells marker (PAX6), trophoblast marker (CDX2), neural crest marker (SOX10, SOX9, and PAX3), and epidermis

marker (TP63 and E-cad). A modified B.C.SB. protocol was used as illustrated. (**B**) Colorimetric maps showing the average fluorescent intensity of PAX6, TP63, SOX10, PAX3, SOX9, CDX2, and E-cad staining. The intensity of each pixel of the images was normalized to the maximum value for each image. n > 20. (C) Plots showing the quantitative average intensity in relation to the distance to the center of the pattern. In these experiments, H9 hES cells were induced using the modified B.C.SB. protocol in E6 medium from day 3 to day 8. Scale bar, 100 μ m.

Figure 6

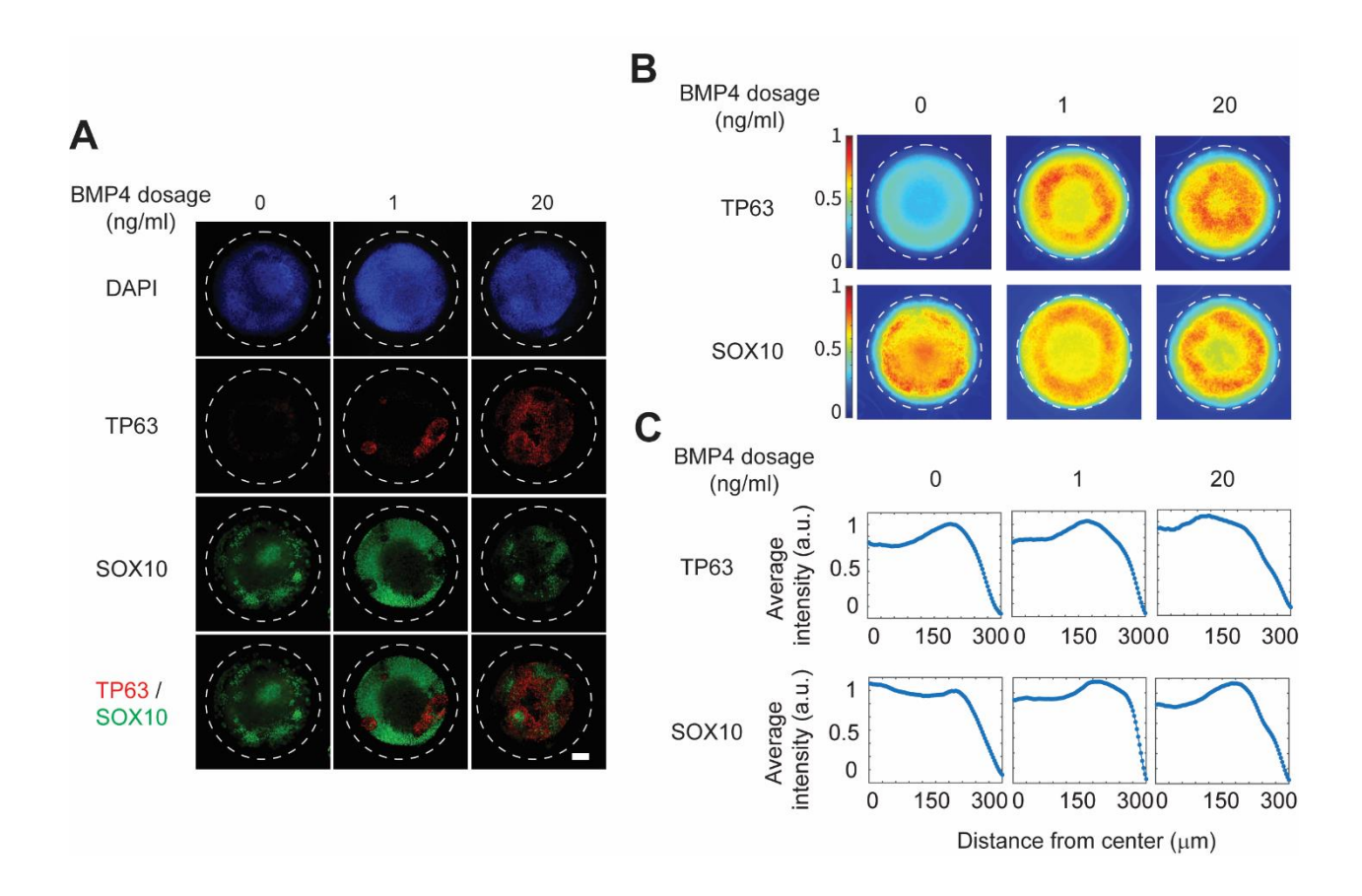


Figure 6. The role of exogenous BMP4 concentration in cell fate decision and pattern formation in ectoderm microtissues. (A) Representative immunofluorescence images showing cell nuclei (DAPI), neural crest marker (SOX10), and epidermis marker (TP63). Cells were differentiated using the B.C.SB. protocol with modified BMP4 concentration as indicated. (B) Corresponding colorimetric maps showing the average fluorescent intensity of SOX10 and TP63 staining. (C) Plots showing the quantitative average intensity in relation to the distance to the center of the pattern. In these experiments, H9 hES cells were induced using the B.C.SB. protocol in E6 medium from day 3 to day 8. Scale bar, 100 μm.

Figure 7

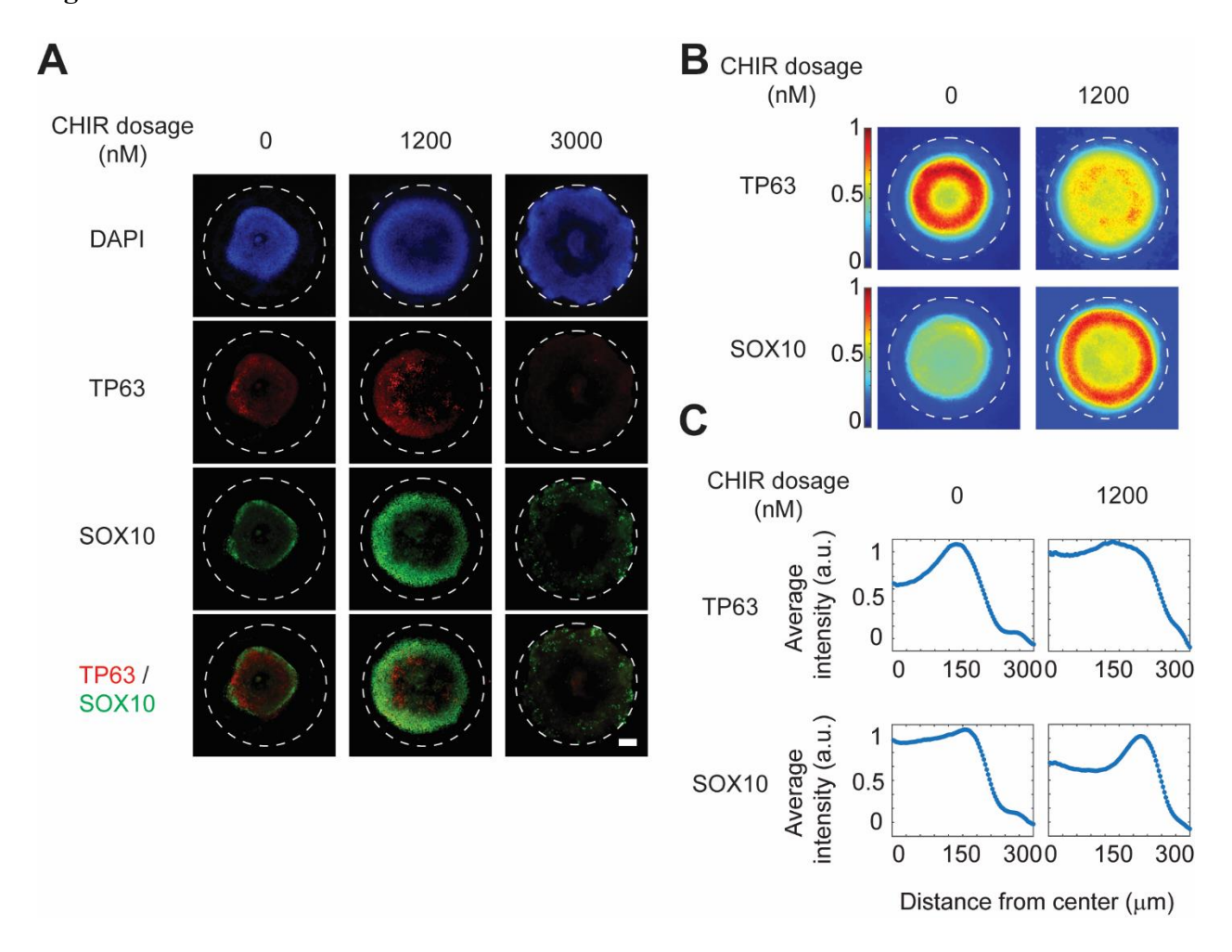


Figure 7. The role of exogenous WNT activation in cell fate decision and pattern formation in ectoderm microtissues. (A) Representative immunofluorescence images showing cell nuclei (DAPI), neural crest marker (SOX10), and epidermis marker (TP63). Cells were differentiated using the B.C.SB. protocol with modified CHIR concentration as indicated. (B) Corresponding colorimetric maps showing the average fluorescent intensity of SOX10 and TP63 staining. (C) Plots showing the quantitative average intensity in relation to the distance to the center of the pattern. In these experiments, H9 hES cells were induced using the B.C.SB. protocol in E6 medium from day 3 to day 8. Scale bar, 100 μm.

Figure 8

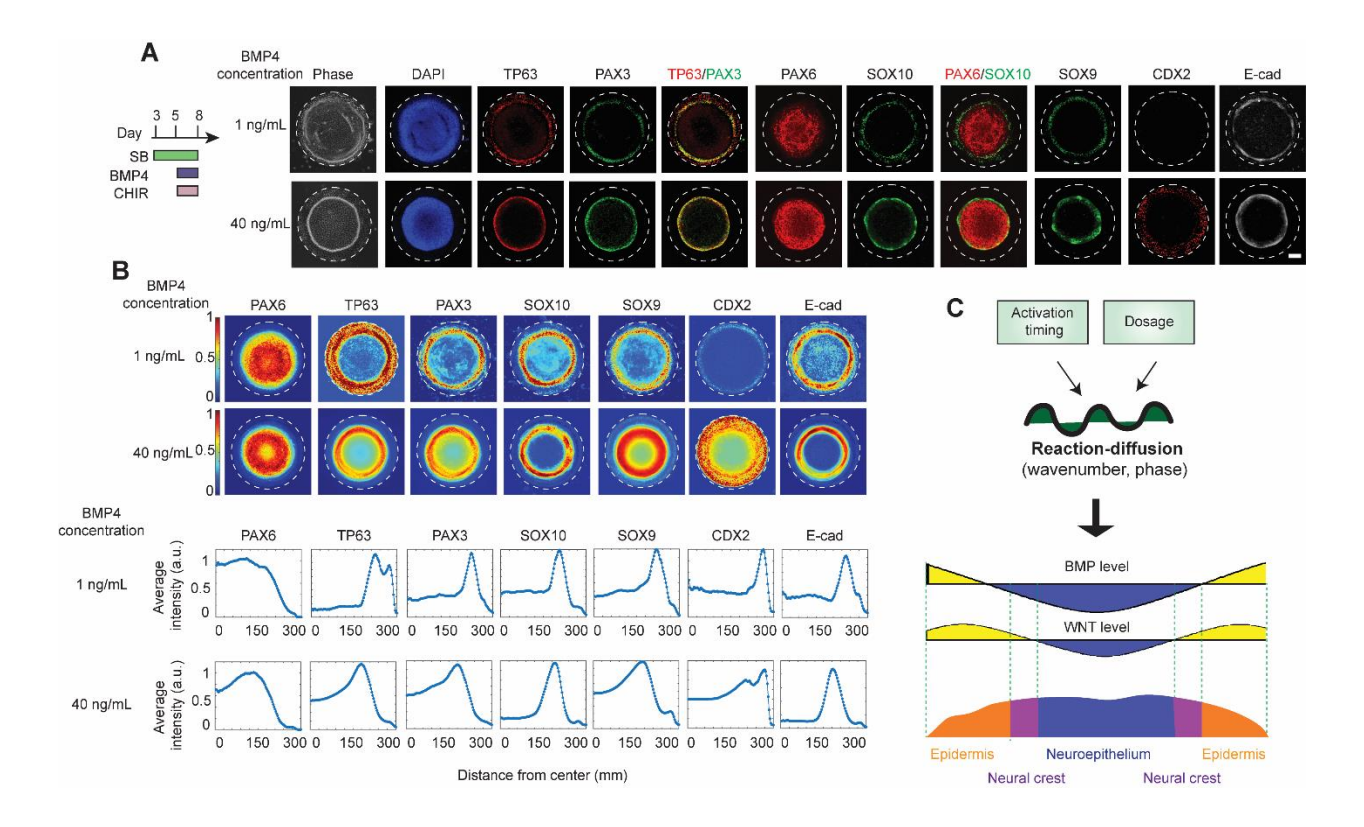


Figure 8. Generation of complete *in vitro* ectoderm microtissues by fine-tuning the BMP signal. (A) Representative phase and fluorescence images showing cell morphology, nuclei (DAPI), neuroepithelial cells marker (PAX6), neural crest marker (SOX10, PAX3, SOX9), trophoblast marker (CDX2), and epidermis marker (TP63, E-cad). A modified B.C.SB. protocol was used as illustrated. (B) Top panel: Colorimetric maps showing the average fluorescent intensity of PAX6, PAX3, SOX9, SOX10, CDX2, TP63, and E-cad staining. The intensity of each pixel of the images was normalized to the maximum value for each image. n > 20. Bottom panel: Plots showing the quantitative average intensity in relation to the distance to the center of the pattern. (C) A schematic showing the reaction-diffusion of both BMP and WNT signals determines the cell fate patterning in ectoderm development. In these experiments, H9 hES cells

were induced using the modified B.C.SB. protocol in E6 medium from day 3 to day 8. Scale bar, $100\ \mu m.$

ACKNOWLEDGMENT

This work is supported in part by the National Science Foundation (CMMI 1662835 and CMMI 1846866 to Y.S.) and the Department of Mechanical and Industrial Engineering at the University of Massachusetts Amherst. The Conte Nanotechnology Cleanroom Lab is acknowledged for support in microfabrication. We also acknowledge the Light Microscopy Facility where confocal microscopy data were collected.

AUTHOR CONTRIBUTIONS

T.X. and Y.S. designed the experiments, T.X. performed all experiments and analyzed data, J.K. and H.Y. developed the reaction-diffusion model. C. P. generated the human induced pluripotent stem cell line. All authors wrote and approved the manuscript.

DECLARATION OF INTERESTS

The authors declare no competing interests.

REFERENCE

- 1. van Ooyen A. Using theoretical models to analyse neural development. **Nat Rev Neurosci**. 2011;12(6):311-26.
- 2. Spemann H, Mangold H. Induction of embryonic primordia by implantation of organizers from a different species. 1923. **Int J Dev Biol**. 2001;45(1):13-38.
- 3. Munoz-Sanjuan I, Brivanlou AH. Neural induction, the default model and embryonic stem cells. **Nature Reviews Neuroscience**. 2002;3(4):271-80.
- 4. Harland R. Neural induction. **Current Opinion in Genetics & Development**. 2000;10(4):357-62.
- 5. Stern CD. Neural induction: old problem, new findings, yet more questions. **Development**. 2005;132(9):2007-21.
- 6. Stern CD. Neural induction: 10 years on since the 'default model'. **Current Opinion in Cell Biology**. 2006;18(6):692-7.
- 7. Gerhart J. Cellular Basis of Morphogenetic Change: Looking Back after 30 Years of Progress on Developmental Signaling Pathways. In: Love AC, editor. Conceptual Change in Biology: Scientific and Philosophical Perspectives on Evolution and Development2015. p. 175-97.
- 8. Zirra A, Wiethoff S, Patani R. Neural Conversion and Patterning of Human Pluripotent Stem Cells: A Developmental Perspective. **Stem Cells International**. 2016.
- 9. Wilson SI, Rydstrom A, Trimborn T, Willert K, Nusse R, Jessell TM, Edlund T. The status of Wnt signalling regulates neural and epidermal fates in the chick embryo. **Nature**. 2001;411(6835):325-30.
- 10. Yoon Y, Huang TT, Tortelote GG, Wakamiya M, Hadjantonakis AK, Behringer RR, Rivera-Perez JA. Extra-embryonic Wnt3 regulates the establishment of the primitive streak in mice. **Developmental Biology**. 2015;403(1):80-8.
- 11. Turner DA, Hayward PC, Baillie-Johnson P, Rue P, Broome R, Faunes F, Arias AM. Wnt/beta-catenin and FGF signalling direct the specification and maintenance of a neuromesodermal axial progenitor in ensembles of mouse embryonic stem cells. **Development**. 2014;141(22):4243-53.
- 12. Li WL, Ding S. Generation of Novel Rat and Human Pluripotent Stem Cells by Reprogramming and Chemical Approaches. **Cellular Programming and Reprogramming: Methods and Protocols**. 2010;636:293-300.
- 13. Copp AJ, Stanier P, Greene ND. Neural tube defects: recent advances, unsolved questions, and controversies. **Lancet Neurol**. 2013;12(8):799-810.
- 14. Warmflash A, Sorre B, Etoc F, Siggia ED, Brivanlou AH. A method to recapitulate early embryonic spatial patterning in human embryonic stem cells. **Nat Methods**. 2014;11(8):847-54.
- 15. Heemskerk I, Burt K, Miller M, Chhabra S, Guerra MC, Liu L, Warmflash A. Rapid changes in morphogen concentration control self-organized patterning in human embryonic stem cells. **Elife**. 2019;8.
- 16. Shao Y, Taniguchi K, Townshend RF, Miki T, Gumucio DL, Fu J. A pluripotent stem cell-based model for post-implantation human amniotic sac development. **Nat Commun**. 2017;8(1):208.
- 17. Xue X, Sun Y, Resto-Irizarry AM, Yuan Y, Aw Yong KM, Zheng Y, Weng S, Shao Y, Chai Y, Studer L, Fu J. Mechanics-guided embryonic patterning of neuroectoderm tissue from human pluripotent stem cells. **Nat Mater**. 2018;17:633-41.

- 18. Mica Y, Lee G, Chambers SM, Tomishima MJ, Studer L. Modeling neural crest induction, melanocyte specification, and disease-related pigmentation defects in hESCs and patient-specific iPSCs. Cell Rep. 2013;3(4):1140-52.
- 19. Xie T, Hawkins J, Sun Y. Traction Force Measurement Using Deformable Microposts. In: Rittié L, editor. Fibrosis: Methods and Protocols. New York, NY: Springer New York; 2017. p. 235-44.
- 20. Barrio RA, Varea C, Aragon JL, Maini PK. A two-dimensional numerical study of spatial pattern formation in interacting Turing systems. **Bull Math Biol**. 1999;61(3):483-505.
- 21. Gomez GA, Prasad MS, Sandhu N, Shelar PB, Leung AW, Garcia-Castro MI. Human neural crest induction by temporal modulation of WNT activation. **Dev Biol**. 2019;449(2):99-106.
- 22. Dincer Z, Piao J, Niu L, Ganat Y, Kriks S, Zimmer B, Shi SH, Tabar V, Studer L. Specification of functional cranial placode derivatives from human pluripotent stem cells. **Cell Rep**. 2013;5(5):1387-402.
- 23. Byrne C, Tainsky M, Fuchs E. Programming gene expression in developing epidermis. **Development**. 1994;120(9):2369-83.
- 24. Xu RH, Chen X, Li DS, Li R, Addicks GC, Glennon C, Zwaka TP, Thomson JA. BMP4 initiates human embryonic stem cell differentiation to trophoblast. **Nature Biotechnology**. 2002;20(12):1261-4.
- 25. Amita M, Adachi K, Alexenko AP, Sinha S, Schust DJ, Schulz LC, Roberts RM, Ezashi T. Complete and unidirectional conversion of human embryonic stem cells to trophoblast by BMP4. **Proc Natl Acad Sci U S A**. 2013;110(13):E1212-E21.
- 26. Basch ML, Bronner-Fraser M, Garcia-Castro MI. Specification of the neural crest occurs during gastrulation and requires Pax7. **Nature**. 2006;441(7090):218-22.
- 27. Pattison JM, Melo SP, Piekos SN, Torkelson JL, Bashkirova E, Mumbach MR, Rajasingh C, Zhen HH, Li LJ, Liaw E, Alber D, Rubin AJ, Shankar G, Bao XM, Chang HY, Khavari PA, Oro AE. Retinoic acid and BMP4 cooperate with p63 to alter chromatin dynamics during surface epithelial commitment. **Nature Genetics**. 2018;50(12):1658-+.
- 28. Haremaki T, Metzger JJ, Rito T, Ozair MZ, Etoc F, Brivanlou AH. Self-organizing neuruloids model developmental aspects of Huntington's disease in the ectodermal compartment. **Nature Biotechnology**. 2019;37(10):1198-208.
- 29. Tchieu J, Zimmer B, Fattahi F, Amin S, Zeltner N, Chen S, Studer L. A Modular Platform for Differentiation of Human PSCs into All Major Ectodermal Lineages. **Cell Stem Cell**. 2017;21(3):399-410.e7.
- 30. Tewary M, Ostblom J, Prochazka L, Zulueta-Coarasa T, Shakiba N, Fernandez-Gonzalez R, Zandstra PW. A stepwise model of Reaction-Diffusion and Positional-Information governs self-organized human peri-gastrulation-like patterning. **Development**. 2017.
- 31. Sick S, Reinker S, Timmer J, Schlake T. WNT and DKK determine hair follicle spacing through a reaction-diffusion mechanism. **Science**. 2006;314(5804):1447-50.
- 32. Turing AM. The chemical basis of morphogenesis. **Bull Math Biol**. 1953;52(1-2):153-97; discussion 19-52.
- 33. Britton G, Heemskerk I, Hodge R, Qutub AA, Warmflash A. A novel self-organizing embryonic stem cell system reveals signaling logic underlying the patterning of human ectoderm. **Development**. 2019:dev.179093.

- 34. Manfrin A, Tabata Y, Paquet ER, Vuaridel AR, Rivest FR, Naef F, Lutolf MP. Engineered signaling centers for the spatially controlled patterning of human pluripotent stem cells. **Nat Meth**. 2019;16(7):640-+.
- 35. Patthey C, Edlund T, Gunhaga L. Wnt-regulated temporal control of BMP exposure directs the choice between neural plate border and epidermal fate. **Development**. 2009;136(1):73-83.
- 36. Raible DW, Ragland JW. Reiterated Wnt and BMP signals in neural crest development. **Seminars in Cell & Developmental Biology**. 2005;16(6):673-82.
- 37. Steventon B, Carmona-Fontaine C, Mayor R. Genetic network during neural crest induction: From cell specification to cell survival. **Seminars in Cell & Developmental Biology**. 2005;16(6):647-54.
- 38. Steventon B, Mayor R. Early neural crest induction requires an initial inhibition of Wnt signals. **Dev Biol**. 2012;365(1):196-207.
- 39. Zhang SC, Wernig M, Duncan ID, Brustle O, Thomson JA. In vitro differentiation of transplantable neural precursors from human embryonic stem cells. **Nature Biotechnology**. 2001;19(12):1129-33.
- 40. Zhou J, Su P, Li D, Tsang S, Duan E, Wang F. High-Efficiency Induction of Neural Conversion in hESCs and hiPSCs with a Single Chemical Inhibitor of TGF-β Superfamily Receptors. **Stem Cells**. 2010;28(10):1741-50.
- 41. Chambers SM, Fasano CA, Papapetrou EP, Tomishima M, Sadelain M, Studer L. Highly efficient neural conversion of human ES and iPS cells by dual inhibition of SMAD signaling. **Nature Biotechnology**. 2009;27(3):275-80.
- 42. Elkabetz Y, Panagiotakos G, Al Shamy G, Socci ND, Tabar V, Studer L. Human ES cell-derived neural rosettes reveal a functionally distinct early neural stem cell stage. **Gene Dev**. 2008;22(2):152-65.
- 43. Knight GT, Lundin BF, Iyer N, Ashton LMT, Sethares WA, Willett RM, Ashton RS. Engineering induction of singular neural rosette emergence within hPSC-derived tissues. **Elife**. 2018:7.
- 44. Lutolf MP, Lauer-Fields JL, Schmoekel HG, Metters AT, Weber FE, Fields GB, Hubbell JA. Synthetic matrix metalloproteinase-sensitive hydrogels for the conduction of tissue regeneration: engineering cell-invasion characteristics. **Proc Natl Acad Sci U S A**. 2003;100(9):5413-8.
- 45. Nakano T, Ando S, Takata N, Kawada M, Muguruma K, Sekiguchi K, Saito K, Yonemura S, Eiraku M, Sasai Y. Self-formation of optic cups and storable stratified neural retina from human ESCs. **Cell Stem Cell**. 2012;10(6):771-85.
- 46. Huch M, Koo BK. Modeling mouse and human development using organoid cultures. **Development**. 2015;142(18):3113-25.
- 47. Lancaster MA, Renner M, Martin CA, Wenzel D, Bicknell LS, Hurles ME, Homfray T, Penninger JM, Jackson AP, Knoblich JA. Cerebral organoids model human brain development and microcephaly. **Nature**. 2013;501(7467):373-9.
- 48. Muguruma K, Nishiyama A, Kawakami H, Hashimoto K, Sasai Y. Self-organization of polarized cerebellar tissue in 3D culture of human pluripotent stem cells. **Cell Rep**. 2015;10(4):537-50.
- 49. Mason JO, Price DJ. Building brains in a dish: Prospects for growing cerebral organoids from stem cells. **Neuroscience**. 2016.